

## WHY BARYONS MATTER: THE KINEMATICS OF DWARF SPHEROIDAL SATELLITES

ALYSON M. BROOKS<sup>1,2</sup>, ADI ZOLOTOV<sup>3</sup>

(Dated: April 18, 2018)

Accepted for publication in *ApJ*

### ABSTRACT

We use high resolution cosmological simulations of Milky Way-mass galaxies that include both baryons and dark matter to show that baryonic physics (energetic feedback from supernovae and subsequent tidal stripping) significantly reduces the dark matter mass in the central regions of luminous satellite galaxies. The reduced central masses of the simulated satellites reproduce the observed internal dynamics of Milky Way and M31 satellites as a function of luminosity. We use these realistic satellites to update predictions for the observed velocity and luminosity functions of satellites around Milky Way-mass galaxies when baryonic effects are accounted for. We also predict that field dwarf galaxies in the same luminosity range as the Milky Way classical satellites should not exhibit velocities as low as the satellites, since the field dwarfs do not experience tidal stripping. Additionally, the early formation times of the satellites compared to field galaxies at the same luminosity may be apparent in the star formation histories of the two populations. Including baryonic physics in Cold Dark Matter models naturally explains the observed low dark matter densities in the Milky Way's dwarf spheroidal population. Our simulations therefore resolve the tension between kinematics predicted in Cold Dark Matter theory and observations of satellites, without invoking alternative forms of dark matter.

### 1. INTRODUCTION

There are fewer small satellite galaxies orbiting our Milky Way (MW) galaxy than predicted by the favored Cold Dark Matter (CDM) cosmological model (Moore et al. 1999; Klypin et al. 1999; Madau et al. 2008; Wadepuhl & Springel 2011; Brooks et al. 2013). Theories often reconcile the discrepancy between the number of observed satellites and CDM predictions by invoking the suppression of star formation in low mass galaxies, for example by UV heating at reionization (e.g., Okamoto et al. 2008). If only the most massive satellites form stars, this can bring the predicted number of luminous satellites down from thousands to tens, in line with observations. Even then a serious problem remains, as the most massive satellites predicted by CDM models are still much too dense compared to what we observe (Boylan-Kolchin et al. 2011, 2012; Wolf & Bullock 2012; Hayashi & Chiba 2012; Tollerud et al. 2012; Martinez 2013). The tension between the observations and the predictions of the CDM model have led some researchers to propose alternative forms of dark matter (e.g., warm or self-interacting) to reduce the central masses of satellites (Macciò & Fontanot 2010; Vogelsberger et al. 2012; Lovell et al. 2012; Anderhalden et al. 2013; Shao et al. 2013; Polisensky & Ricotti 2013). However, the highest resolution simulations available to date to study the internal properties of satellites include only the dark matter (DM) component of galaxies, neglecting the effects of baryons (e.g., Diemand et al. 2007; Springel et al. 2008; Boylan-Kolchin et al. 2012).

Zolotov et al. (2012) recently examined how baryons impact the DM structure in satellites around a MW-mass galaxy. They demonstrate that supernova (SN) feedback reduces the central DM densities of satellites with  $M_* \gtrsim 10^7 M_\odot$  before infall (see also Governato et al. 2012). However, SN feedback alone is not enough to bring the observed densities of satellites in line with observations. After infall, the presence of a baryonic disk in the host galaxy increases the mass loss rate for all satellites via tidal stripping (Zolotov et al. 2012; Arraki et al. 2012). This tidal effect is particularly strong for those satellites that enter with cored DM halos (Peñarrubia et al. 2010), further increasing the discrepancy in the central masses predicted by DM+baryon and DM-only simulations. Previous studies have invoked tidal stripping after infall to reduce the DM masses of satellite galaxies (Gnedin et al. 1999; Taylor & Babul 2001; Hayashi et al. 2003; Kazantzidis et al. 2004; Kravtsov et al. 2004; Read et al. 2006; Sales et al. 2007b; Muñoz et al. 2008; D'Onghia et al. 2010; Choi et al. 2009; Collins et al. 2011). The additional central mass present in the parent halo of a baryonic run (due to the fact that baryons can cool to the center, unlike DM) lead to an enhanced tidal force not found in DM-only simulations, leading to enhanced stripping. These earlier works examined the evolution in the densities of satellites using idealized models, because cosmological simulations were unable to achieve similar resolutions until recently.

The results of these idealized models can be used to parametrize the stripping of mass based on the orbital history of a satellite. However, even after considering the additional tidal stripping that should occur in a cosmologically motivated population of DM-only satellites, studies still could not reproduce a  $z = 0$  satellite population that matches the observed MW satellite kinematics. Not enough mass is stripped from the most massive satellites to bring them in line with the kinematics observed in the most luminous satellites of the MW

<sup>1</sup>Department of Astronomy, University of Wisconsin-Madison, 475 N. Charter St., Madison, WI 53706

<sup>2</sup>Department of Physics & Astronomy, Rutgers, The State University of New Jersey, 136 Frelinghuysen Rd, Piscataway, NJ 08854; abrooks@physics.rutgers.edu

<sup>3</sup>Racah Institute of Physics, The Hebrew University, Jerusalem, Israel 91904; adizolotov@gmail.com

(Read et al. 2006; D’Onghia et al. 2010). Read et al. (2006) concluded that the most massive satellites would need to have central density slopes shallower than NFW models to undergo enough stripping to make the theoretical and observational masses consistent. This is because subhalos become more prone to tidal forces as their density slopes become less steep (Hayashi et al. 2003; Kazantzidis et al. 2004; Peñarrubia et al. 2010).

Zolotov et al. (2012) are the first to use cosmological simulations to probe the combined reduction in mass from both DM core creation and tidal stripping in the satellite population around a MW-mass galaxy. In this paper, we use a complementary sample of satellites to extend the analysis presented in Zolotov et al. (2012) and further explore the observational consequences of the model. We show that this model can, for the first time in fully cosmological simulations of MW-mass galaxies, reproduce the observed kinematics of dwarf Spheroidal (dSph) satellites in  $L^*$  galaxies at  $z = 0$ . We use our results to interpret the observed trend and scatter in the dynamics of the MW and M31 dSphs. We also demonstrate that the inclusion of baryonic physics leads to destruction of a number of luminous satellites that otherwise survive in DM-only simulations, and make new predictions for the surviving subhalo mass and luminosity functions of  $L^*$  galaxies. Finally, we compare our simulated dSphs to simulated field dwarfs of the same luminosity, and make predictions for observable differences in the two populations.

## 2. THE SIMULATIONS

The simulations that we use here are drawn from Zolotov et al. (2012, hereafter Z12), and we refer the reader to that paper for full details of the simulations. Briefly, two halos with virial masses of  $7 \times 10^{11} M_\odot$  and  $8 \times 10^{11} M_\odot$  at  $z = 0$  were run with and without baryons. The DM-only simulations were run with PKDGRAV (Stadel 2001), while the simulations with baryons were run with PKDGRAV’s N-Body + Smoothed Particle Hydrodynamics (SPH) successor, GASOLINE (Wadsley et al. 2004). In the SPH runs, gas can cool via primordial and metal lines following Shen et al. (2010). A prescription for creation and destruction of  $H_2$  is implemented following Christensen et al. (2012), and star formation is tied directly to the presence of  $H_2$  gas. A uniform UV background turns on at  $z = 9$ , mimicking reionization (Haardt & Madau 2001). Supernovae deposit  $10^{51}$  ergs of thermal energy into the surrounding gas following the “blastwave” scheme described in Stinson et al. (2006).

### 2.1. Satellite Sample

In Z12, the satellite sample was identified using the SPH simulations. That is, the sample included only satellites in the luminosity range of the “classical” MW dSphs, with  $M_V$  brighter than  $-8$ , and within the virial radius of the main SPH halo, i.e., within  $\sim 240$  kpc of the center of the parent halo. We then identified the matching counterparts of these surviving, luminous subhalos in the DM-only run. In this work we take an alternative approach, and instead identify our sample based first on the surviving subhalos of the DM-only simulations, and then search for their matching counterparts in the SPH runs. In addition, since most of the classical dSphs could

be observed even beyond 240 kpc, we extend our search beyond the defined virial radius. In this paper, we have chosen to include all halos with  $v_{max} > 15$  km/s at  $z = 0$  that are within 300 kpc of the main halos.

This new satellite selection yields 62 DM-only satellites combined between the two MW-mass halos. This is more satellites than were presented in Z12, for three reasons. First, extending the search to 300 kpc nearly doubles the number of satellites in one of our halos, though adds only two satellites in the other. Second, there are more satellites in the DM-only run than the SPH run at  $z = 0$ . This is due to baryonic processes, which more efficiently destroy satellites in the SPH run. As we’ll show in Section 4, this destruction is most effective for satellites with small pericentric radii. The primary destruction mechanisms are tidal heating and disk shocking, in which the SPH satellite passes very close to or through the parent galaxy’s disk, which does not exist in the DM-only run. Our two MW-mass halos have a combined total of eight satellites that survive in the DM-only runs, but which are destroyed in the SPH runs by  $z = 0$  (six of which are brighter than  $M_V = -8$ ). Third, the luminous satellites selected in Z12 had DM-only counterparts that generally had  $v_{max}$  at infall,  $v_{@infall}$ , greater than 25 km/s. Our new satellite selection introduces lower mass halos.

The primary benefit of our new satellite selection is that it allows us to highlight in detail the discrepancies that occur between a DM-only run and a baryonic run due to the inclusion of baryonic physics. Not only can we explore the source of the discrepancies, but demonstrate the erroneous conclusions that would result if one tries to use DM-only simulations to match observational results.

### 2.2. Baryonic Evolution with Mass

Our concern in this paper is with luminous satellites bright enough to be considered classical dSphs, with  $M_V$  brighter than  $-8$ . These satellites are bright enough that their detection should currently be nearly complete out to 300 kpc in the MW (Tollerud et al. 2008; Walsh et al. 2009). Z12 showed that the  $z = 0$  satellite populations of both simulated galaxies are in good agreement with the MW and M31 satellite luminosity functions, from  $-8 < M_V < -15$ . Despite the inclusion of more satellites when searching out to 300 kpc, only one satellite in each of the two MW-mass simulations is added that is bright enough to be considered a classical dSph, and thus does not significantly alter the luminosity functions. The remaining satellites that have now been included from beyond the virial radius would be too faint to identify given their distances and current observational limits. As we discuss in the next paragraph, the lower mass halos that we’ve added are fainter than the classical dSphs, and therefore do not alter the luminosity functions.

The circular velocities of classical dSphs in the MW and M31 are typically below 20 km/s, suggesting that our subhalo sample with  $v_{max}$  down to 15 km/s might host luminous dSphs. However, we have found that our lowest mass halos do not form enough stars to be considered a classical dwarf. We investigate this further by identifying  $v_{@infall}$  for all of our halos. Assuming that  $v_{@infall}$  corresponds to the highest mass that the subhalo had, prior to being tidally stripped after accretion onto the main halo, it should be the best predictor of a subhalo’s luminosity (e.g., Kravtsov 2010; Rashkov et al.

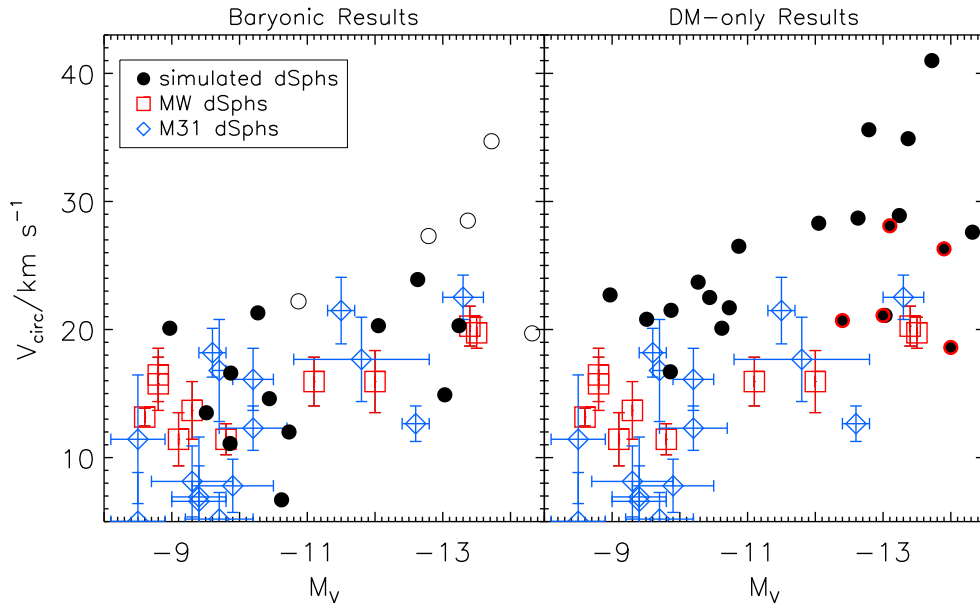


FIG. 1.— Observational data from the MW and M31 satellites compared to the satellite populations of two simulated MW-mass hosts. *Left:*  $v_{max}$  at  $z = 0$  for the SPH satellites as a function of their  $V$ -band magnitude. The solid circles are gas-free at  $z = 0$ , and are true dSph analogs. The empty circles are SPH satellites that still contain gas. The empty red squares and empty blue diamonds are  $v_c$  at the half light radii for MW and M31 dSphs, respectively. *Right:*  $v_{max}$  at  $z = 0$  for the satellites in the DM-only runs as a function of the  $V$ -band magnitude or their matched SPH counterpart. The baryonic simulated dSphs have the same range of magnitudes and velocities as the observed dSphs, while the high  $v_{max}$  values of the DM-only simulations are inconsistent with the observations. The circles with red rings indicate satellites for which the SPH counterpart has been completely tidally destroyed.

2012; Hearin et al. 2013). Indeed, Z12 found a tight correlation between  $v_{@infall}$  and the stellar mass of the subhalos in these simulations.

We use AHF (Knollmann & Knebe 2009; Gill et al. 2004) to identify halos and subhalos at every output step, and trace back the most massive progenitor of each satellite. We find that the faintest halos are also the lowest mass at infall. All of our halos with  $v_{@infall} < 20$  km/s have stellar masses below  $10^5 M_\odot$ , and  $M_V$  fainter than  $-7$ . All of our SPH satellites brighter than  $M_V = -8$  have  $v_{@infall} > 20$  km/s. However, there is some stochasticity in halos with  $20 < v_{@infall} < 25$  km/s. In this mass range, some dwarfs are bright enough to be considered classical dSphs, but some are too faint.

The nature of the star formation in the subhalos varies with mass. All of the more massive, luminous satellites with  $v_{@infall} > 25$  km/s are able to retain gas until infall, allowing their star formation histories (SFHs) to extend at least until infall. On the other hand, halos with  $v_{@infall} \lesssim 25$  km/s typically lose their gas prior to accretion onto the parent halo. Heating from the uniform UV background, combined with early star formation and SN feedback, removes a substantial amount of gas from these low mass halos, leaving them gas poor. These halos lose 10 – 90 times more mass in gas than stars formed by the time of their accretion. The remaining gas has low surface densities and is inefficient at producing stars. The low level of star formation that can occur prior to infall is relatively constant rather than stochastic.

Halos with  $v_{@infall} > 25$  km/s are able to retain more of their gas for longer, allowing them to have extended SFHs (in line with observational data,

see Grebel & Gallagher 2004; Dellenbusch et al. 2008; Weisz et al. 2011). In halos with  $v_{@infall} > 30$  km/s, the SFHs tend to be episodic and bursty, unlike the lower mass satellites. With their deeper potential wells, the more massive halos achieve an initially higher star formation rate (SFR) than the lower mass halos as gas cools in the central galaxy. The subsequent SN feedback following a burst of star formation heats the surrounding gas, shutting off star formation for a period of time until the gas can again cool and continue with another burst. The bursty SFHs in the most massive halos lead to DM core creation prior to infall (see also Read & Gilmore 2005; Macciò et al. 2012b; Pontzen & Governato 2012; Teyssier et al. 2012b; Peñarrubia et al. 2012; Garrison-Kimmel et al. 2013).<sup>1</sup>

Many subhalos lose most of their gas after infall and are gas-free by  $z = 0$ .<sup>2</sup> While some subhalos lose their gas nearly instantly at infall, some are capable of retaining their gas for an extended time, and even having a low level of star formation. However, the SFRs become strongly suppressed after infall, and no subhalo continues to undergo the bursty star formation that contributes to DM core creation.

### 3. INTERPRETING OBSERVED DWARF SPHEROIDALS

<sup>1</sup> Note that some authors have suggested that processes such as dynamical friction or angular momentum transfer are also responsible for DM core creation (e.g., El-Zant et al. 2001; Tonini et al. 2006; Del Popolo 2009).

<sup>2</sup> Satellites that retain gas until  $z = 0$  may be artificially gas-rich, due to inefficient stripping of gas in this implementation of SPH (Agertz et al. 2007).

Below we discuss the observational properties of the Milky Way and M31 dSphs in light of results that show that baryonic effects can reduce the central DM masses of luminous satellites that infall onto a  $\sim L^*$  galaxy.

### 3.1. Satellite Kinematics at Redshift 0

Figure 1 shows  $v_{max}$  of the simulated satellites as a function of  $M_V$ . The simulated SPH satellites are shown in the left panel, while the DM-only satellites are shown in the right panel. The  $v_{max}$  values for the simulated gas-free satellites in the SPH run span the range of 6-24 km/s, consistent with  $v_c$  results for MW and M31 dSphs (red and blue symbols, respectively). In contrast, all but 2 of the DM-only counterparts have  $v_{max} > 20$  km/s, grossly inconsistent with the MW and M31 dSph data.

The filled circles in the left panel of Figure 1 show the gas-free SPH satellites (dSph analogs). Satellites that still retain gas are shown for completeness as empty circles. Plotted with the simulation data are the observed circular velocities at the half light radii for dSphs with  $M_V$  brighter than  $-8$  in both the MW and M31. The MW data is drawn from the compilation of McConnachie (2012). The M31 data is taken from table 5 in Collins et al. (2013a), where overlapping results with Tollerud et al. (2012) are weighted based on the quality of the observations. For the observational data,  $v_c(r_{1/2}) = \sqrt{3\sigma^2}$ , where  $\sigma$  is the line of sight stellar velocity dispersion, and  $r_{1/2}$  is the half-light radius of the dSph. Walker et al. (2009) and Wolf et al. (2010) have shown that assumptions about isotropy are minimized at  $r_{1/2}$ , making the masses determined at  $r_{1/2}$  the most robust. Because most dwarfs show flat  $\sigma$  profiles (Walker et al. 2009), it is assumed that  $v_c(r_{1/2})$  is roughly equal to  $v_{max}$ . In any case, the half-light radii are  $\lesssim 1$  kpc for all of the observed dSphs. Our measurements for the simulated satellites are upper limits to the values derived at typical half light radii, as the rotation curves of these satellites either peak or continue to rise at 1 kpc.

Since the line of sight stellar velocity dispersions are the most direct comparison to observations, we show in Figure 2 a comparison of our simulated stellar dispersions to the observations. The same simulated SPH satellites shown in the left panel of Figure 1 are shown in Figure 2. We have chosen a random line of sight. Similar to the observational data, we found that the stellar dispersions are relatively constant with radius. Hence, in Figure 2 we plot the value of the dispersion measured at the half light radius, just as in the observations. We find that the dispersions are in good agreement with the range of observed dispersions. This demonstrates that, although Figure 1 is an indirect comparison of the mass enclosed between the observations and simulations, a more direct comparison measured at similar radii also confirms that the simulations with baryons are able to reproduce the observational results.

The right panel of Figure 1 shows the satellites in the DM-only simulation compared to the observational data. Each DM-only subhalo is assigned the  $V$ -band magnitude of its matched SPH satellite counterpart. As we discuss in Section 4, some of the DM-only subhalos survive to  $z = 0$ , but their counterparts in the SPH run are destroyed. These subhalos have been indicated by red

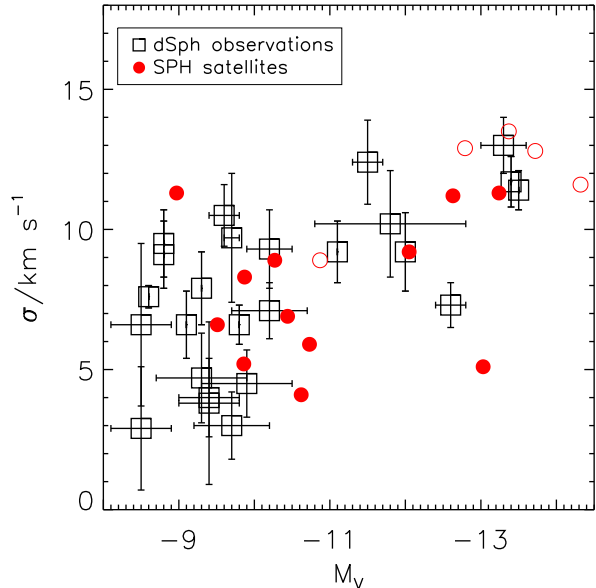


FIG. 2.— Stellar line-of-sight velocity dispersions,  $\sigma$ , in satellites measured at the half light radius, as a function of  $V$ -band magnitude. Data for MW and M31 dSphs are now shown collectively as empty squares, and the simulated satellites are in red. As in Figure 1, the solid circles are gas-free SPH satellites at  $z = 0$ , and are true dSph analogs. The empty circles are SPH satellites that still contain gas. This plot is similar to the left panel of Figure 1, but is a more robust test of the SPH simulations since it directly compares to the observational data.

rings surrounding the data points. For those subhalos, we assign the luminosity of the matched SPH subhalo at the time it is accreted to the parent halo, well prior to its disruption. All of these destroyed satellites are brighter than  $M_V < -12$ , so there are many more bright DM-only subhalos than in the SPH run.

In Figures 1 and 2, we restrict ourselves to examining the sample of halos that host classical, luminous dSphs. This neglects just over half of the subhalos that we have identified with  $v_{max}(z = 0) > 15$  km/s and within 300 kpc, because they are fainter than  $M_V = -8$  where the observational data is incomplete (Tollerud et al. 2008; Walsh et al. 2009). At the bright end, we also wish to ignore those satellites that are Magellanic Cloud analogs. Boylan-Kolchin et al. (2012) assign Magellanic status to those halos that had  $v_{@infall} > 60$  km/s and  $v_{max}(z = 0) > 40$  km/s. This removes one subhalo from our sample. However, two additional satellites (one in each halo) have  $v_{@infall} > 40$  km/s, but were accreted less than 25 Myr prior to  $z = 0$ . We remove these from the sample as well, as they are clearly dwarf Irregular (dIrr) analogs rather than dSphs.

Previous studies using DM-only simulations have found that subhalos simulated in a CDM-context are significantly more dense than observations of the MW dSphs suggest (Boylan-Kolchin et al. 2011, 2012; Wolf & Bullock 2012; Hayashi & Chiba 2012; Rodríguez-Puebla et al. 2013). However, when baryonic effects are modeled self-consistently, as they are here, the kinematics of simulated satellites are well-matched to the observed kinematics of dSph satellites.

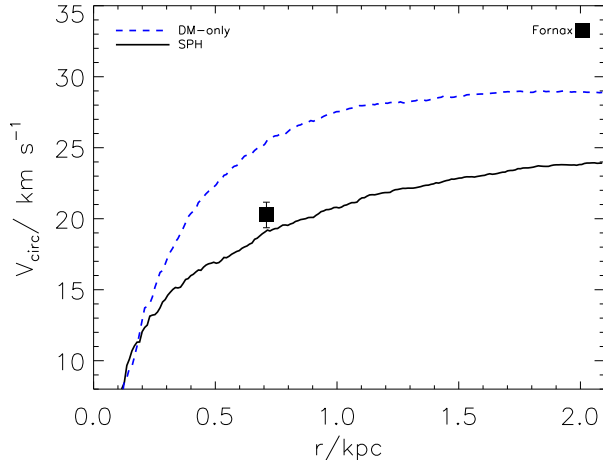


FIG. 3.— The  $z = 0$  rotation curves of a simulated satellite and its DM-only counterpart. The  $v_c$  for Fornax is over-plotted, based on the data in Walker et al. (2009). The combination of SN feedback (before infall) and tidal stripping (after infall) substantially lower the  $v_c$  of the SPH satellite by  $z = 0$ , and is in good agreement with the observed  $v_c$  of Fornax.

Figure 1 demonstrates that DM-only simulations over-predict the central DM masses of satellite galaxies, and explains why results from such simulations yield satellite populations that are inconsistent with the kinematics of the MW dSphs. An explicit example of the difference in kinematics for a bright satellites produced in a DM-only context compared with the same satellite in a baryonic simulation is shown in Figure 3. The total rotation curve (DM and baryonic mass) for an SPH simulated subhalo is shown in Figure 3, which closely matches the derived  $v_c$  at the half light radius of Fornax, along with the rotation curve for the same subhalo in a DM-only run without baryons. The DM-only satellite clearly over-predicts the central mass of this satellite. For almost all of our satellites, the *DM-only runs produce satellites with 2 – 4 times more mass in the central 1 kpc than their SPH counterparts*.

It is common when making predictions for the properties of subhalos within the CDM model to associate the most massive DM-only subhalos at infall with the most luminous satellites at  $z = 0$  (e.g., Koposov et al. 2009; Boylan-Kolchin et al. 2011, 2012), i.e., an abundance matching technique. Indeed, the most massive subhalos in the DM-only runs in this work are matched to the most luminous satellites in the SPH runs at infall (as shown in Z12). However, SPH satellites experience evolution that DM-only runs do not account for. It is therefore incorrect to assume that the central masses of DM-only subhalos should predict the observed masses in the inner regions of luminous subhalos.

### 3.2. The Scatter in $v_c$

A long-standing puzzle in the observed data shown in Figure 1 is that some of the bright MW dSphs with  $M_V \sim -13$  have similar  $v_c$  values to some of the much fainter galaxies with  $M_V \sim -8$ . In the field, galaxies display a clear trend of increasing stellar mass with halo mass (e.g., Behroozi et al. 2010; Moster et al. 2012; Leauthaud et al. 2012; Behroozi et al. 2013), yet satellites that span two orders of magnitude in luminosity

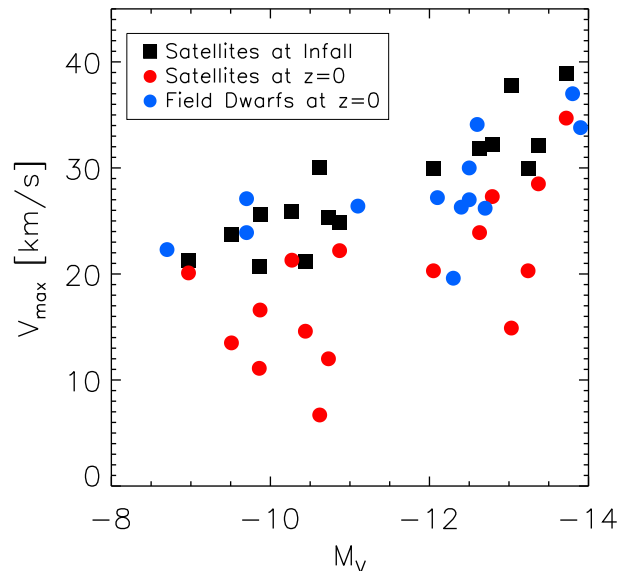


FIG. 4.— The  $v_{max}$  values of simulated dwarfs. The black squares show the simulated satellites at the time of their accretion. The red circles show the satellites'  $v_{max}$  at  $z = 0$  (as in Figure 1). The blue circles show  $v_{max}$  at  $z = 0$  for simulated field dwarfs in the same luminosity range as the classical dSphs (discussed further in Section 5).

seem to show no trend in their central  $v_c$  with mass. The comparable velocities of Draco ( $M_V = -8.8$ ), and Fornax ( $M_V = -13.4$ ), for example, have led Peñarrubia et al. (2008) to conclude that Draco formed in a halo 5 times more massive than Fornax, despite being 70 times fainter.

The simulated SPH satellites shown in Figure 1 follow a similar trend to the observed MW and M31 dSphs; at  $z = 0$  simulated satellites with  $M_V = -9$  can have comparable kinematics to satellites with  $M_V = -13$ . At infall, however, SPH satellites follow an increasing trend of stellar mass with halo mass, with  $M_* \propto M_{vir}^2$ . This is shown in Figure 4. The trend seen for satellites at infall (black squares) and in the field at  $z = 0$  (blue circles; discussed further in Section 5) is erased in the subsequent tidal evolution of the satellites, resulting in the scatter observed at  $z = 0$  (red circles).

Since both SPH and DM-only satellites undergo tidal stripping, one might expect that SPH and DM-only satellites would display a similar scatter in  $v_c$  at  $z = 0$ . However, when DM-only satellites are matched to the stellar mass of their SPH counterparts, DM-only satellites still show a trend of increasing  $v_{max}$  with luminosity at  $z = 0$ , unlike satellites simulated with baryons. This can be seen in the right panel of Figure 1, particularly when one neglects those satellites that have destroyed SPH counterparts (with red rings). The DM-only satellites with destroyed SPH counterparts do undergo much more tidal stripping than other subhalos, but in the presence of a disk this should have led to their total disruption. When the DM-only satellites with surviving SPH counterparts are considered, there is a trend of increasing  $v_{max}$  with luminosity.

Two effects lead to the divergence in the scatter of  $v_c$  between SPH and DM-only satellites. First, the presence

of a baryonic disk<sup>4</sup> in the host galaxy enhances the rate of mass lost at each pericentric passage for all SPH satellites. In essence, because the baryonic simulations have a component (gas) that can cool to the center of the parent halo, there is more mass sitting at the center of the parent halo, which leads to stronger tidal forces. Using the same set of simulations as this paper, we showed in Z12 (see Figure 6 in Z12) that SPH satellites undergo a larger reduction in their central circular velocity after infall than DM-only satellites. In that work, we showed that this effect is partially due to the baryonic disk in the SPH simulated host, and is increasingly significant with increasing time after infall and for satellites with smaller pericenters (see also Peñarrubia et al. 2010). The variation in infall times and orbital pericenters results in the large spread of  $v_c$  values for simulated SPH satellites fainter than  $M_V \sim -12$ , similar to the observational data in Figure 1. Because DM cannot cool to form a disk, the primary host in the DM-only simulation has no central disk component, and the low-mass DM-only subhalos that come near the central regions of the host do not experience enhanced tidal stripping. Hence, they do not reproduce the observed scatter in  $v_c$  at low masses (or equivalently, at low  $M_V$ ).

The second effect at play in creating the scatter in  $v_c$  for SPH satellites is that the influence of a baryonic disk is especially strong for satellites with shallow DM density profiles, like the SPH satellites in our sample brighter than  $M_V \sim -12$ . A shallower density profile means that the halo has a lower binding energy, which exacerbates the amount of central mass lost in the most luminous subhalos due to tidal stripping. The satellites fainter than  $M_V = -12$  have not had enough star formation to create shallow DM density profiles or large DM cores (Peñarrubia et al. 2012), so the reduction in mass is strictly due to tidal stripping. For the brighter satellites, tidal stripping effects are even more severe due to the presence of a shallow DM density profile. The reduction in DM density due to DM core creation alone is insufficient to reduce the central densities of the brighter satellites to the low  $v_c$  values observed (see also Garrison-Kimmel et al. 2013). However, the presence of a DM core in the satellite leads to enhanced tidal stripping that contributes to lowering the central  $v_c$  of these satellites to under 25 km/s. The result of these processes is that satellites across the luminosity range appear to have similar masses at  $z = 0$ . Without the effect of the disk, and with their steep density profiles, DM-only satellites experience overall less mass loss for a given orbit, and therefore tidal effects do not introduce a large scatter in their  $v_c$ .

#### 4. THE ROLE OF TIDES

It is well established that dSphs are DM dominated galaxies (e.g., Mateo 1998; Simon & Geha 2007; McConnachie 2012). Given that the baryonic processes described here all lead to decreasing the DM mass in a satellite before any stars are stripped, a natural question is whether these processes can still result in galaxies that are as DM dominated as the observed dSphs in the Local

<sup>4</sup> Note that the baryons need not be in a disk. Any concentration of baryons, even in a spherical bulge, still leads to more tidal stripping than in the DM-only case (Chang et al. 2013).

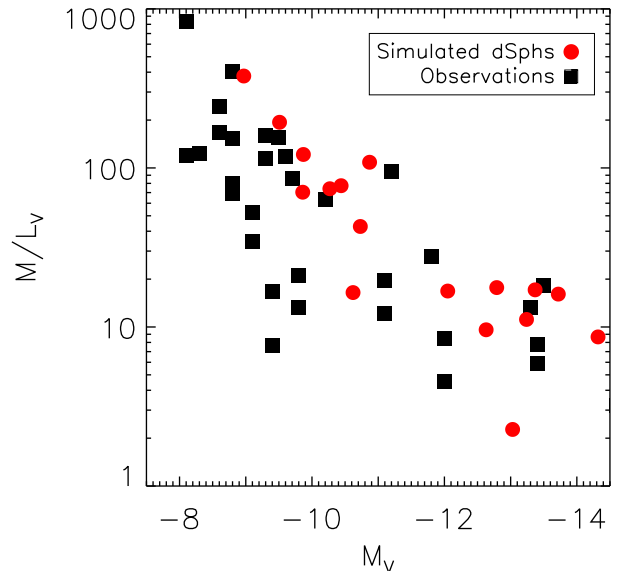


FIG. 5.— The mass-to-light ratio,  $M/L$ , within the half light radius for the simulated SPH satellites (red circles) as a function of  $V$ -band magnitude. Data from dSphs in the MW (McConnachie 2012) and M31 (Tollerud et al. 2012; Collins et al. 2013a; Tollerud et al. 2013) are shown as black squares. The simulations match the observed trend of increasing  $M/L$  ratio with decreasing luminosity.

Group.

Figure 5 shows the mass-to-light ( $M/L_V$ ) ratios within the half light radius for the baryonic simulations as a function of  $M_V$  (red circles). The solid black squares are observed dSphs. The MW data is taken from tables 3 and 4 in McConnachie (2012), while the Andromeda data is compiled from Tollerud et al. (2012), Collins et al. (2013a), and Tollerud et al. (2013). The simulations match the observed trend of increasing  $M/L$  ratio with decreasing luminosity.

The driving property behind this  $M/L$  trend is the relation of stellar mass to halo mass for the simulations,  $M_{star} \propto M_{halo}^2$ . As discussed above, while some subhalos lose substantial amounts of DM after infall, most lose only a factor of 2–4 from their central regions. This small change is not enough to significantly alter the  $M/L$  ratio. Hence, the trend in  $M/L$  ratio is driven by the luminosity as a function of halo mass<sup>3</sup> instead of mass loss.

#### 4.1. Orbital Dependence

Z12 explored the difference in mass tidally stripped after infall as a function of pericentric distance,  $R_{peri}$ . Their figure 6 shows that significant discrepancies between DM-only and baryonic runs can occur for  $R_{peri} \lesssim$

<sup>3</sup> For stellar masses above  $10^6 M_\odot$ , this relation is in agreement with commonly adopted relations in the literature, (e.g., Koposov et al. 2009; Kravtsov 2010; Rashkov et al. 2012; Sales et al. 2013). At lower stellar masses, these same authors find a slightly steeper relation, with  $M_{star}$  scaling as  $M_{halo}^{2.5-3}$ . This difference between our simulation relation and derived relations has little to no impact on the results in this paper, but may explain the tendency for the fainter simulated satellites to lie systematically to slightly higher  $M_V$  than observations in Figure 5.

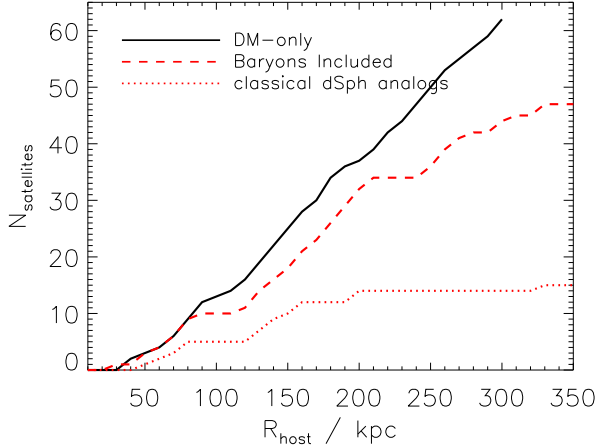


FIG. 6.— The cumulative distribution of radial distance from the galaxy center for the subhalos. The solid black line shows the results for the DM-only runs, while the dashed red line is for the baryonic runs. Destruction of subhalos in the presence of a baryonic disk leads to a depletion of the SPH satellites compared to the DM-only runs.

40 kpc due to the stronger tidal forces present when baryons cool to the center of the halo. We have verified that the  $R_{peri}$  values between matched counterparts in the DM-only and baryonic simulations do not show any global differences. For example, one might expect that the SPH satellites could have smaller  $R_{peri}$  if adiabatic contraction occurred in the parent halo, but we find no evidence for this.

In this section we discuss two effects that, in addition to tidal stripping, are likely to be important in understanding the evolution of satellites – tidal heating and disk shocking. Within  $\sim 20$  kpc of the galaxy center, tidal heating and disk shocking are the dominant processes that lead to mass loss from subhalos (see D’Onghia et al. 2010), and were not discussed in Z12. Tidal heating is efficient for eccentric orbits and can destroy satellites faster than tidal stripping (Gnedin et al. 1999). Disk shocking occurs when the subhalos pass through the dense baryonic disk. The rapidly varying gravitational field adds energy to the subhalos, altering the structure, and quickly leading to dissolution (Ostriker et al. 1972).

In our simulations, 8 of the original 62 DM-only subhalos do not have a surviving SPH counterpart at  $z = 0$ . Six of these subhalos have pericentric passages that take them within 30 kpc of the galaxy center,  $16 < R_{peri}/kpc < 29$ . For comparison, the radial extent of the parent halos’ disks are  $7 < r/kpc < 10$  at  $z = 1$ , and  $15 < r/kpc < 20$  at  $z = 0$ . The other two disrupted subhalos are subject to the cosmological context of the simulations, encountering fly-bys with nearby halos that lead to their destruction prior to accretion onto the main halo. The destruction of these two halos emphasizes that, while the main culprit that reduces the subhalo population is the disk of the parent halo, interactions with nearby galaxies can also deplete the subhalo population (see also Kravtsov et al. 2004).

The radial distribution of the subhalos at  $z = 0$  is shown in Figure 6. Figure 6 shows that there is only one surviving subhalo within 30 kpc of the galaxy cen-

ter in the baryonic run at  $z = 0$ , (and no bright, classical dSphs interior to 40 kpc, dotted red line), consistent with the results in both D’Onghia et al. (2010), and Romano-Díaz et al. (2010). This is also consistent with the bright satellite distribution in the Milky Way, where only Sagittarius is observed within 30 kpc, and is in the process of being disrupted.

The satellite distribution in the DM-only run and baryonic runs is very similar out to  $\sim 80$  kpc, and then begins to diverge (black solid line and red dashed line). There is a tendency for the SPH satellites in the outer halo to reside at larger distances than their DM-only counterparts. This is consistent with later accretion times in the SPH runs than the DM-only runs, as also seen by Schewtschenko & Macciò (2011).

All but one of the surviving DM-only satellites that have destroyed SPH counterparts are further than 80 kpc from the galaxy center at  $z = 0$ . In other words, most of the surviving DM-only subhalos with destroyed counterparts are found beyond  $\sim 80$  kpc at  $z = 0$ , but were within 30 kpc at some point in their orbital history. Thus, when considering the halos within a DM-only run that may have been completely destroyed by baryonic effects, the entire orbital history needs to be accounted for.

In summary, the presence of a disk acts not only to reduce the overall masses of the SPH subhalos via tidal stripping, but it can also reduce the number of satellites overall. We quantify these combined effects further in the next section.

#### 4.2. The Velocity and Luminosity Functions

Figure 7 shows the combined effects of mass loss and complete disruption on the resulting velocity and luminosity functions of the satellites. Solid circles show the combined results for the two DM-only simulations, while the open circles show the combined results for the two SPH simulations. The left hand panel shows the  $v_{max}$  function. In this panel we include all 62 of the subhalos identified in the DM-only runs that have  $v_{max}(z = 0) > 15$  km/s and are within 300 kpc of the main halos.

The  $v_{max}$  function can differ quite dramatically between the SPH and DM-only satellites, due to multiple physical effects. First, in a luminous subhalo ( $M_V$  brighter than  $-12$ ), SN feedback can induce DM core creation. DM is pushed out of roughly the central kpc (Pontzen & Governato 2012). This redistribution of the DM acts to lower  $v_{max}$  in the baryonic run to  $\sim 90\%$  of the value in their DM-only counterparts. Second, the presence of a disk leads to enhanced tidal stripping for *all* of the subhalos. This process depends on infall time and orbital history for any given satellite, and therefore does not yield a smooth trend of mass loss as function of  $v_{max}$ , but is instead stochastic. Third, the number of subhalos at a given  $v_{max}$  is reduced because some of the baryonic subhalos are destroyed entirely. While this final effect removes halos entirely, the first two effects instead shuffle the  $v_{max}$  distribution from that found in the DM-only runs. This redistribution always acts to move subhalos to lower  $v_{max}$ , so that the cumulative number above a fixed  $v_{max}$  is always lower in the baryonic runs compared to the DM-only runs. The top plot in the left panel of Figure 7 shows that, at any given mass or  $v_{max}$ , there are roughly half as many subhalos in the baryonic run

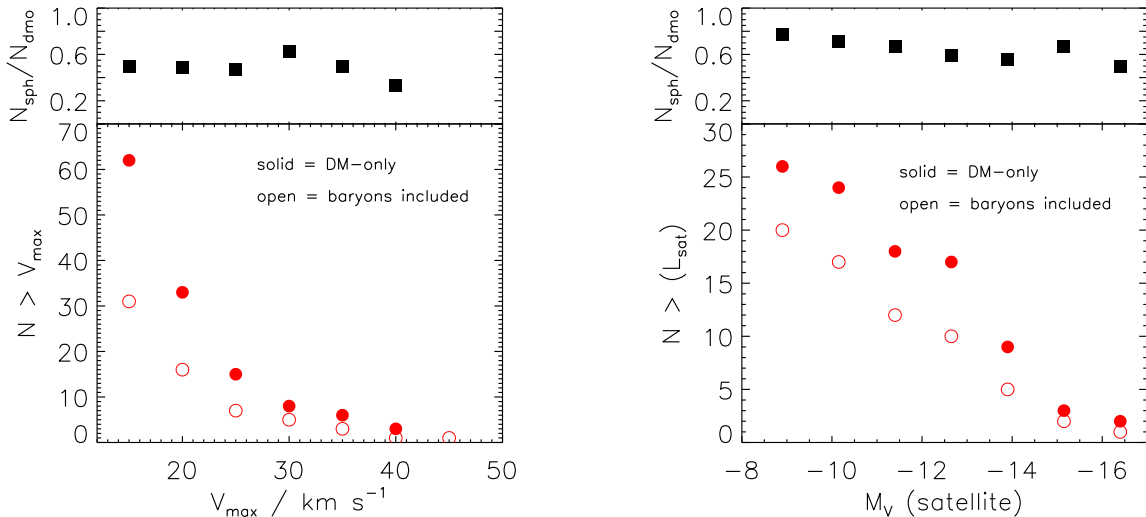


FIG. 7.— The  $z = 0$  cumulative satellite velocity functions and luminosity functions. Solid circles show the combined results for the two DM-only simulations, while the open circles show the combined results for the two SPH simulations. *Left*: The  $v_{max}$  function for the satellites. All 62 subhalos identified in the DM-only runs with  $v_{max}(z = 0) > 15\text{km/s}$  and within 300 kpc of the main halos are shown here, compared to surviving SPH counterparts in the same velocity range. The combined effects discussed in this paper (DM core creation, enhanced tidal stripping due to the presence of a disk, and tidal heating/disk shocking) all lead to a reduced number of subhalos at a given  $v_{max}$  in the baryonic run compared to the DM-only runs. The top plot shows that the number of subhalos is reduced by roughly a factor of two across the entire subhalo mass range we consider here. *Right*: The cumulative luminosity function for the satellites. In this panel we use only the luminous satellites where observations are complete,  $M_V$  brighter than  $-8$ . We also include dIrr/Magellanic Cloud analogs. The luminosity function is altered when satellites are completely destroyed in the baryonic runs. The top plot shows that there are roughly 1/3 fewer luminous satellites in the baryonic runs compared to the DM-only runs.

compared the the DM-only run (see also D’Onghia et al. 2010). Note that this reduction leads many of the SPH subhalos to have  $v_{max} < 10\text{ km/s}$  at  $z = 0$ , and are not shown on this plot.

The right hand panel of Figure 7 shows the luminosity function of the satellites. In this panel we neglect the faint halos ( $M_V$  fainter than  $-8$ ) where observational tests are incomplete, so there are fewer than half as many subhalos in the right panel as in the left panel. However, unlike Figures 1 and 5 that exclude 3 bright dIrr/Magellanic Cloud analogs, we include the bright dIrrs here in order to demonstrate that discrepancies exist between the SPH and DM-only runs even up to the brightest, most massive satellites. Unlike the  $v_{max}$  function, where processes could remove DM mass and shift surviving subhalos to lower  $v_{max}$ , there is no shifting to lower luminosities that can occur. In other words, tidal stripping can remove up to 90% of the DM mass in a subhalo, but leave the tightly bound stellar content in place (Muñoz et al. 2008; Peñarrubia et al. 2008; Libeskind et al. 2011; Chang et al. 2013). This alters the  $v_{max}$  function, but not the luminosity function. Instead, when tidal effects begin to finally disrupt the stellar content, the subhalo is soon thereafter completely destroyed. Hence, the primary effect that alters the luminosity function of the subhalos is complete destruction. Six luminous satellites, or roughly 1/3 of the luminous satellites, are destroyed in the baryonic runs that survive in the DM-only runs (the two other destroyed satellites are fainter than  $M_V = -8$ ). Hence, the top plot of the right panel in Figure 7 shows that the baryonic runs contain roughly 2/3 the satellites compared to the DM-only runs.

## 5. COMPARISON TO FIELD DWARFS

Mass loss due to tidal effects is the essential component to reproduce the range of observed  $v_c$  in dSphs. We demonstrate this in Figure 8. The observational data for the satellites (empty squares) shown in Figure 8 is derived again from dispersions measured at the half light radii, as in Figure 1. We again plot our simulated satellites, but this time we show  $v_c(1\text{kpc})$  rather than  $v_{max}$  as before. Also shown as solid squares are observed field galaxies, all measured at 1kpc, from LITTLE THINGS (Oh, *private comm.*), Côté et al. (2000, for the Sagittarius dwarf Irregular galaxy), and McGaugh et al. (2007, for DDO 154). The LITTLE THINGS data have been corrected for asymmetric drift, and include only galaxies for which a tilted ring analysis could be done. We have used a larger sample of seven “zoom-in” simulations (including the two simulations from which our simulated satellite data is drawn) to identify isolated (non-satellite) dwarf galaxies in the same luminosity range of the classical dSphs (blue circles). Five simulations have the same resolution as the satellite results ( $\epsilon = 174\text{pc}$ ), but two have even higher resolutions ( $\epsilon = 87\text{pc}$ ).

The values for the observed dwarf field galaxies in Figure 8 (solid black squares) represent  $v_{rot}$  measured at  $\sim 1\text{ kpc}$ . Unlike the simulated dSphs sample, where  $v_{max}$  is comparable to  $v_c$  measured at 1 kpc ( $v_{1\text{kpc}}$ ),  $v_{max}$  of the simulated field dwarfs can occur at much larger radii (3 – 11 kpc in the luminosity range examined here,  $-8 > M_V > -14$ ). Since the half light radii of observed dSphs are typically 1 kpc or less, we measure  $v_{1\text{kpc}}$  for the field dwarfs for the most direct comparison. Figure 8 demonstrates that the mass enclosed in the field sample is systematically higher than that in observed dSphs. While observed dSphs all have  $v_c < 25\text{km/s}$ , the



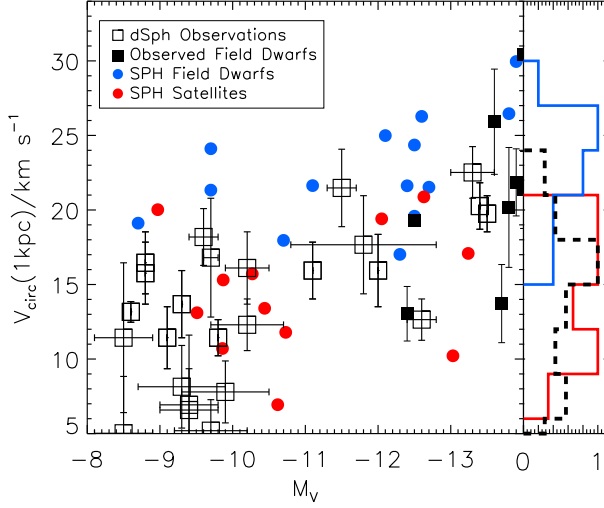


FIG. 8.— The empty squares show observational data for the MW and M31 dSphs ( $v_c$  at the half light radii), as in Figure 1. The remaining data points in this plot show  $v_c$  at 1kpc. Simulated dwarf field galaxies are shown by blue circles, and simulated satellites are shown by red circles. Values for  $v_c$  at 1kpc in observed dwarf field galaxies (Oh, *private comm.*; Côté et al. 2000; McGaugh et al. 2007) are shown by black squares. Histograms of the  $v_c$  distributions are shown on the right of the plot. The blue line shows the  $v_c$  for the simulated field dwarfs, the red line shows the  $v_c$  for the simulated satellites, while the dashed black line shows the  $v_c$  distribution for the observed dSphs for comparison. Although dwarf field galaxies may span the same magnitude range as the observed satellites, they systematically reside at higher  $v_c$  than observed in dSphs. Tidal stripping is required to remove enough mass in these luminous dwarfs in order to reach the range of observed  $v_c$  in dSphs.

field dwarfs in the same luminosity range instead have  $15 < v_c < 30$  km/s. Using  $v_{max}$  for the field dwarfs instead of  $v_{1kpc}$  would shift this range to 20-40 km/s (see Figure 4).

In general, the observed  $v_{rot}$  for field dwarfs at 1 kpc is in agreement with our simulated field galaxies. Two of the LITTLE THINGS dwarfs lie below the range we predict, but we stress that the data is preliminary, and that these same set of simulations generally match the central densities of the THINGS and LITTLE THINGS sample at 500pc (Oh et al. 2011; Governato et al. 2012). We also note that there is a strong luminosity bias, so that only galaxies brighter than  $M_V = -12$  have been observed. We leave it to future work to more closely evaluate whether our simulated field dwarf sample matches the velocity function of observed dwarfs (e.g., Papastergis et al. 2011; Ferrero et al. 2012). For now, we predict the field sample should lie systematically to higher  $v_c$  values than dSphs (or dwarf Ellipticals assuming this trend continues to brighter satellites).

Figure 4 demonstrates that the  $v_{max}$  of the satellites at the time of their accretion is in the range  $20 < v_{max} < 40$  km/s, comparable to the range of the simulated field dwarf galaxies at  $z = 0$  presented here. Hence, the satellites start off with comparable masses to field dwarfs, but it is their subsequent mass loss through tidal stripping that results in the range of lower  $v_c$  values that is actually observed. In other words, while there exist field galaxies with  $v_{1kpc}$  comparable to observed dSphs (in the 15 – 25

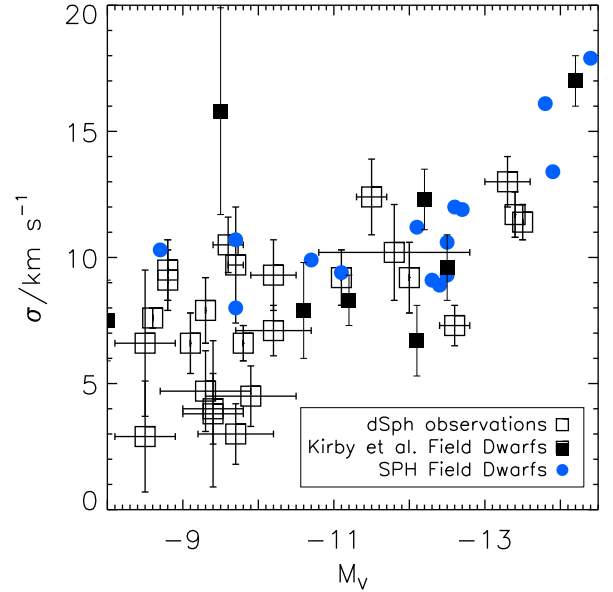


FIG. 9.— Stellar line-of-sight velocity dispersions,  $\sigma$ , in dwarfs measured at the half light radius, as a function of  $V$ -band magnitude. Data for MW and M31 dSphs are shown collectively as empty squares. The solid squares are dispersion values measured in field dwarfs by Kirby et al. (2014), who found that the dispersions of the field galaxies and the satellites show no significant offset. Solid blue circles are simulated SPH field dwarfs, and are in agreement with the results of Kirby et al. (2014). The field dwarfs do not seem to have dispersions that span to the lowest values observed in the satellites ( $\sigma < 5$  km/s).

km/s range), we predict that field galaxies in this luminosity range should not span the full range of low  $v_c$  that are observed in dSphs. The exception to this rule might occur if field galaxies have previously undergone a fly-through with a more massive galaxy (Sales et al. 2007a; Oman et al. 2013; Teyssier et al. 2012a). However, these galaxies should presumably be fewer in number than field galaxies that have avoided strong interactions, so that a population of satellite galaxies should show systematically lower central masses ( $v_{1kpc}$ ) than field galaxies at a fixed luminosity.

A recent measurement of stellar velocity dispersion in Kirby et al. (2014) allows us to begin to test the tidal scenario. Kirby et al. (2014) measured velocity dispersions within the half light radius for a number of field dwarfs in the same luminosity range as the dSphs. They found that there is no significant difference in the dispersions of field and satellite dwarfs. We compare our simulated field galaxies to the Kirby et al. (2014) sample in Figure 9. Like the field observations, the dispersions of our simulated field dwarfs also show no significant offset from the dSph observations. However, we note that, in both the observations and simulations, field galaxies never seem to span to the lowest  $\sigma$  values observed in the satellites.

Kirby et al. (2014) removed any rotational component from the kinematics, but found little rotation in their sample. Likewise, our simulated field dwarfs show little net rotation at the small radii probed in Figures 8 and 9. At face value, this suggests that both the field and satel-

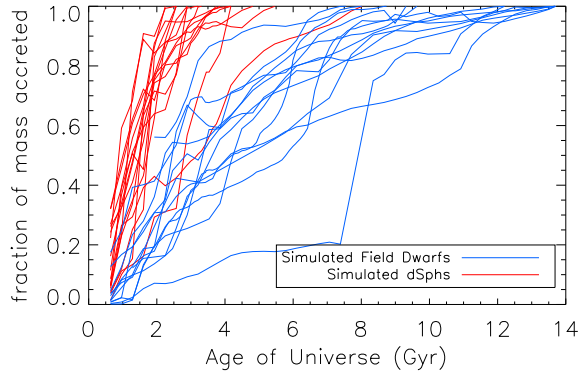


FIG. 10.— The mass accretion histories of the simulated SPH satellites (red lines) and the simulated dwarf field sample (blue lines), both in the magnitude range  $-14 < M_V < -8$ . The MAH of the satellites is truncated at the time of their infall onto their parent halo. Satellites tend to be accreted at  $z > 1$ , meaning that they reach, at much higher  $z$ , similar  $v_{max}$  values to the field dwarfs at  $z = 0$ . This also means that they reside in more concentrated halos than typical field dwarfs observed at  $z = 0$ .

lites galaxies are dispersion dominated, and have similar  $v_c$  values (or at least that the field dwarfs do not show significantly larger  $v_c$  values than the satellites). Figure 9 demonstrates that our simulated field dwarfs agree with this picture *when dispersions are measured within the half light radius of the galaxies*. The half light radii of these dwarfs are generally much smaller than 1 kpc. On the other hand, Figure 8 demonstrates that a clearer separation in  $v_c$  begins to appear between the two samples as further radii are probed. We predict that future measurements that can probe out to 1 kpc or more will begin to see this offset that has been created by tidal stripping in the satellites.

The fact that the observed satellites and observed field dwarfs have an overlapping range of  $v_c$  values raises a finer point. A naive conclusion might then be that satellites and field dwarfs at a fixed luminosity were born in similar halos. However, this is not the case. As was just stated, the  $v_{max}$  range of the dSphs *at infall* is comparable to the  $v_{max}$  range of field dwarfs *at  $z=0$*  (see Figure 4), and this is an important distinction. The dSphs reached this  $v_{max}$  at much higher redshift than the field sample.

We demonstrate this in Figure 10, where we show the mass accretion histories (MAH) of our simulated satellites and simulated field dwarfs. These simulated dwarfs all lie in the magnitude range  $-14 < M_V < -8$ , so the satellite sample excludes three dIrr/Magellanic Cloud analogs that tended to fall in at recent times. The MAH of the satellites is truncated at the infall time onto the parent halo for clarity (the masses decline after infall, as we have emphasized in this paper). Most satellites in our sample were accreted at  $z > 1$ . One of the consequences of the fact that satellites have an earlier MAH than field dwarfs is that satellites reside in much denser halos than typical field dwarfs at  $z = 0$ . This is a natural consequence of galaxy formation in the CDM cosmological model, as galaxies that form at higher redshifts are more concentrated (Wechsler et al. 2002; Zhao et al. 2003), and early forming subhalos are found preferentially closer to the center of MW-mass galaxies (Diemand et al. 2005; Moore et al. 2006).

The more concentrated halos and deeper potential wells of the satellites compared to the field dwarfs could be manifest in the star formation histories (SFHs) of the two populations. Assuming that SFHs are truncated or significantly lowered after infall of the satellites due to ram pressure stripping of their gas, the cumulative SFHs of the satellites should be biased to higher  $z$  than field dwarfs, which exhibit continued SF all the way to  $z = 0$ . We verified that this is the case; the simulated dSphs show an earlier peak in their cumulative SFHs than the simulated field dwarfs. A plot of the cumulative SFH looks very similar to the MAH shown in Figure 10, so we do not show them here. We will instead present them in a comparison to Local Group data in a future paper (Weisz et al., *in prep.*).

Observationally, there is a hint that dSphs do have a faster rise in SF at early times compared to dIrr in the ANGST data (Weisz et al. 2011). However, ANGST also contains the dynamically young group M81 (Nichols & Bland-Hawthorn 2013), and within errors the cumulative SFHs of the dSphs and dIrr are indistinguishable. New work comparing the cumulative SFHs of dSphs and dIrr in the Local Group suggest a larger difference, with the SFHs of dSphs peaking closer to  $z = 1$  (Weisz et al., *in prep.*), though again the error bars are large. We also note that some MW dSphs show evidence for very recent SF, within the last  $\sim 1$  Gyr (Grebel & Gallagher 2004; Dellenbusch et al. 2008). This is not excluded by the model, but depends strongly on infall time for any given halo, how long a satellite is able to retain gas after infall, and whether any re-accretion occurs (de Boer et al. 2013). However, even if a few dSphs continue SF to low  $z$ , the population as a whole should show much earlier SF on average, according to our model, than a population of field dwarfs at similar luminosities.

Thus, although field dwarf masses may be similar to dSphs at a fixed luminosity, this does not mean that tidal processes in the dSphs are unimportant. Rather, satellites should have formed in denser halos at high  $z$ . The most luminous dSphs had  $v_{max}$  up to 40 km/s at infall (typically  $z > 1$ ), and it is only through tidal stripping (aided by DM cored density profiles in the most luminous satellites) that they reach values below 25 km/s at  $z = 0$ . We predict that only satellite galaxies that have experienced substantial mass loss via tidal stripping should reach the lowest observed  $v_c$  values at a fixed luminosity (see also Collins et al. 2013b).

## 6. DISCUSSION

### 6.1. The Existence of Cores in dSphs

The reduction in  $v_c$  across all luminosities in our satellites simulated with baryonic physics is primarily due to tidal stripping, with the ability of baryons to cool to the central region of the host halo leading to stronger tidal forces on the satellites than in a DM-only run. However, for the brightest satellites the mass loss is aided by the presence of a shallow DM density profile created by stellar feedback prior to accretion of the satellite onto the main halo. Below we discuss the observational evidence for cores in dSphs.

Most attempts to measure the central density slopes of dSphs have relied on using the spherical Jeans equations (e.g., Gilmore et al. 2007), but the mass and anisotropy

of the stellar orbits are degenerate in the Jeans model, making the results highly dependent on adopted assumptions (Evans et al. 2009). Recent works (Wolf & Bullock 2012; Hayashi & Chiba 2012; Richardson & Fairbairn 2013) have attempted to overcome this issue by searching for maximum likelihoods in parameter space, but still adopt Jeans modeling. Schwarzschild modeling avoids some of the assumptions inherent in Jeans modeling, and has been applied to Fornax and Sculptor, with the conclusion that both have cored DM density profiles (Jardel & Gebhardt 2012; Jardel et al. 2013; Jardel & Gebhardt 2013; Breddels et al. 2013).

Alternatively, dSphs with multiple stellar populations that span varying radii allow a direct fit to two independent derivations of the mass, avoiding assumptions about a mass model or isotropy. Studies using this method (Walker & Peñarrubia 2011; Amorisco & Evans 2012; Battaglia et al. 2008; Agnello & Evans 2012) conclude that both Fornax (with slope measured out to  $\sim 1$  kpc) and Sculptor (measured interior to 500 pc) favor cored density profiles, and exclude cuspy density profiles at high significance. It has also been argued that the fact that Fornax’s globular cluster orbits have not decayed by dynamical friction requires a cored DM profile (Goerdt et al. 2006; Cole et al. 2012). A similar argument was recently made regarding observed stellar substructure in Sextans (Lora et al. 2013).

Overall, it has been argued both that the dSphs may all have a universal density profile (e.g., Walker et al. 2009), and that they don’t (e.g., Collins et al. 2013b). There is also no accepted conclusion regarding whether any given dSph has a cuspy or cored density profile. Despite the results above that favor a cored profile in Fornax, other studies have found it to be consistent with a cusp (Strigari et al. 2010; Breddels & Helmi 2013). This is not necessarily surprising given the difficulty and biases involved in modeling these systems (Battaglia et al. 2013). For example, the results may depend sensitively on whether the line-of-sight views the minor or major axis of the dSph (Kowalczyk et al. 2013; Laporte et al. 2013; Wojtak et al. 2013). Future galaxy-galaxy lensing experiments may be able to put additional constraints on the density profiles of satellites (Li et al. 2013).

The presence of cored density profiles at radii less than  $\sim 500$  pc in satellites fainter than  $M_V \sim -12$  (as seen in Sculptor by Walker & Peñarrubia 2011) is not ruled out by our simulations, as we do not resolve this region. Although satellites in this luminosity range are unlikely to have had enough stellar feedback to produce large, kpc-sized cores (Peñarrubia et al. 2012; Garrison-Kimmel et al. 2013), it is possible that lower energies may lower the density profiles at much smaller radii. Higher resolution simulations are necessary to determine if small ( $< 500$  pc) DM cores should exist in lower luminosity satellites.

Despite the lack of conclusive evidence for cored profiles in dSphs, it is already clear that the overall concentrations of the MW dSph population are lower than predicted by CDM DM-only simulations (Boylan-Kolchin et al. 2012; Wolf & Bullock 2012; Hayashi & Chiba 2012). The lowered densities of our satellites simulated with both DM and baryons are consistent with these observational results. The substantial reduction in the overall normalization of the central

DM densities of satellites due to the presence of a disk will lead to a reduced DM annihilation signal. Deeper searches for DM annihilation could help to constrain the central masses of these objects.

## 6.2. Are Alternative DM Models Necessary?

The discrepancies between various observational characteristics of the MW’s dSph population and DM-only simulation predictions have led some theorists to suggest alternative models to CDM, such as Warm DM (WDM, Bode et al. 2001; Boyarsky et al. 2009; Tikhonov et al. 2009) or self-interacting DM (SIDM, Spergel & Steinhardt 2000; Buckley & Fox 2010; Tulin et al. 2013; Vogelsberger & Zavala 2013). We have shown in this paper that baryonic effects have the potential to resolve one of the problems of the CDM model, the “too big to fail” problem (Boylan-Kolchin et al. 2012). In Brooks et al. (2013) we argued that these same baryonic effects not only bring the masses, but also the numbers of massive satellites into agreement with observations, potentially solving the “missing satellites” problem (Klypin et al. 1999; Moore et al. 1999). We discuss here the implications for a couple of popular alternative DM models.

First, we note that the effect of the enhanced tidal stripping in the presence of baryons may alter the mass and luminosity functions in a similar way to Warm DM (WDM) models. Nierenberg et al. (2013) examined both the satellite luminosity and mass functions of observed luminous satellites in galaxies with masses comparable to and greater than the MW between  $0.1 < z < 0.8$ . They compared their observational results to the predicted mass and luminosity functions for three different CDM semi-analytic models, and one WDM semi-analytic model. Despite varying physical prescriptions, none of the three CDM models was a good match to the data, which instead favored the WDM model results (though see Macciò et al. 2012a; Kang et al. 2013; Viel et al. 2013; Schneider et al. 2013). The WDM mass and luminosity functions were typically reduced by a factor  $\sim 2$ -3 relative to the CDM predictions. This is consistent with our reductions when considering baryonic effects, though we caution that we examine only two halos. Future work with a statistical sample of galaxies will put better constraints on the role of baryons. However, the current results suggest that baryonic effects can reduce the number of subhalos in a comparable way to WDM models, requiring future work to identify predictions to rule out or favor a specific DM model. In particular, we plan to run these same simulations in a WDM scenario with baryons, in order to quantify whether CDM+baryons can be observationally distinguished from WDM+baryons using dSphs.

The primarily effect of WDM is to erase substructure below the free-streaming scale (Angulo et al. 2013; Benson et al. 2013). Above this scale, the main difference of WDM halos from CDM halos is a lower concentration due to later formation times (Destri et al. 2013; Lovell et al. 2013). The later formation times yield SFHs that peak later in WDM models (Herpich et al. 2013; Libeskind et al. 2013). It remains to be seen whether the presence of baryons yields a stronger effect in the lower concentrations of WDM halos. However, SIDM should already lead to DM core formation, without the

need for baryons. Tension currently exists over the necessary cross-section for DM interaction that can yield core sizes as observed in dwarfs compared to halo shapes of galaxy clusters (Peter et al. 2013; Rocha et al. 2013; Zavala et al. 2013). To date, no SIDM simulation has included baryons. Again, future work is needed to test whether the combination of SIDM and baryons can reproduce observed trends in dSphs.

Before these simulations with WDM+baryons or SIDM+baryons can be completed, there are already hints that SIDM might be necessary in field dwarfs. As discussed above, dwarfs with stellar masses below  $\sim 10^7 M_\odot$  should not be able to create large DM density cores through stellar feedback. Yet the observed  $v_{rot}$  in galaxies at these low masses seems to be consistently lower than the expected  $v_c$  in CDM DM-only simulations (Papastergis et al. 2011; Ferrero et al. 2012). If this discrepancy is not able to be reconciled by considering baryonic effects, or by a full consideration of observational biases, then it suggests some other mechanism might be necessary to reduce the central masses of these field dwarfs. SIDM would be a natural candidate.

## 7. CONCLUSIONS

We have demonstrated that simulations that account for the effects of SN feedback and enhanced tidal stripping on satellites result in a satellite population whose kinematic properties match the observed properties of the Milky Way and M31 satellites. Our findings are in sharp contrast to studies using DM-only simulations, which over-predict the central masses of satellites in comparison to observations.

By directly comparing the properties of simulated satellites that include gas hydrodynamics to the same satellites in DM-only simulations, we find:

1. The majority of satellites simulated with DM-only have  $v_{max} > 20$  km/s, grossly inconsistent with the observed kinematics of the Local Group dSph population. We note that this is despite using simulated parent halos that are on the low side of the allowed range for the MW. Although lowering the mass of the MW has been suggested as a solution to the “too big to fail” problem (Vera-Ciro et al. 2013; Sawala et al. 2012), our DM-only halos with virial masses of  $7 - 8 \times 10^{11} M_\odot$  fail to produce a satellite population with kinematics consistent with observations. In contrast, gas-free satellites simulated with baryonic physics have  $v_{max}$  values in the range of 6–24 km/s, matching the observed values of Local Group dSphs. The reduction in  $v_{max}$  in these simulated galaxies is due to the combined effect of SN feedback on very luminous satellites (brighter than  $M_V = -12$ ) and enhanced mass stripping for satellites across all luminosities in the presence of the parent galaxy’s disk.
2. We find that the velocity dispersions of the simulated satellites are in good agreement with the range of observed dispersions in the MW and M31 dSph satellites.
3. DM-only simulations produce satellites with 2–4 times more mass in the central 1 kpc than satellites simulated with baryonic physics.

4. Satellites simulated with baryons and DM reproduce the observed scatter  $v_c$  for dSphs, while satellites simulated with DM-only do not. A tight  $v_{max}$ –luminosity relation exists for the satellites prior to infall. After infall, the tidal effects of the baryonic disk in the host galaxy lead to large scatter based on the range of infall times and orbital pericenters of the satellites.
5. Simulations that included baryonic physics have 1/3 fewer satellites that survive to  $z=0$  than DM-only simulations. Six out of the eight DM-only satellites that have no surviving SPH counterpart have orbits that bring them within the central 30 kpc of their host galaxy. It seems therefore likely that the destruction of satellites in the baryonic run is due to tidal heating and shocking at the interface of the disk in the parent halo. These effects alter the predicted luminosity functions for satellites at  $z = 0$  from the DM-only case.
6. Increased mass loss in tides for the satellites in the simulation with baryons, combined with total destruction of 1/3 of the satellites, shifts the velocity function of satellites at  $z = 0$  relative to the DM-only predictions. The shift always acts to move satellites toward lower  $v_{max}$  values than in the DM-only run. At any given  $v_{max}$ , we find there are 50% fewer satellites expected when baryonic effects are included.
7. Simulated field dwarf galaxies have systematically higher  $v_{max}$  and  $v_{1kpc}$  values at  $z = 0$  than satellite galaxies in the same luminosity range. Tidal forces are necessary for satellites to reach the low  $v_c$  values observed. Preliminary results from observed field dwarfs suggest our simulated field dwarf velocities are consistent with observations in the local Universe.
8. We find that simulated field dwarfs have similar velocity dispersions to simulated satellite galaxies when compared at the half light radii. These findings reproduce the recent observations of (Kirby et al. 2014).
9. Satellite galaxies have mass assembly histories that peak at higher redshifts than isolated field dwarf galaxies in the same luminosity range. These early assemblies are likely to be manifest in the cumulative SFHs of the dSphs vs dIrrs.

We thank Michael Boylan-Kolchin, Alan McConnachie, Louie Strigari, Matt Walker, and Beth Willman for useful discussions. We thank Se-Heon Oh for supplying velocity data for Little THINGS galaxies. AB acknowledges support from The Grainger Foundation. AZ acknowledges support from the Lady Davis Foundation. This material is based upon work supported in part by the National Science Foundation Grant No. 1066293 and the hospitality of the Aspen Center for Physics. AZ’s work was partially supported by the ISF grant 6/08, by GIF grant G-1052-104.7/2009, by the DFG grant STE1869/1-1.GE625/15-1. Resources

supporting this work were provided by the NASA High-End Computing (HEC) Program through the NASA Advanced Supercomputing (NAS) Division at Ames

Research Center. We thank Charlotte Christensen, Fabio Governato, Tom Quinn, Sijing Shen, and James Wadsley for use of the GASOLINE code and simulations.

## REFERENCES

- Agertz, O. et al. 2007, *MNRAS*, 380, 963
- Agnello, A., & Evans, N. W. 2012, ArXiv e-prints
- Amorisco, N. C., & Evans, N. W. 2012, *MNRAS*, 419, 184
- Anderhalden, D., Schneider, A., Macciò, A. V., Diemand, J., & Bertone, G. 2013, *JCAP*, 3, 14
- Angulo, R. E., Hahn, O., & Abel, T. 2013, *MNRAS*, 434, 3337
- Arraki, K. S., Klypin, A., More, S., & Trujillo-Gomez, S. 2012, ArXiv e-prints
- Battaglia, G., Helmi, A., & Breddels, M. 2013, ArXiv e-prints
- Battaglia, G., Helmi, A., Tolstoy, E., Irwin, M., Hill, V., & Jablonka, P. 2008, *ApJ*, 681, L13
- Behroozi, P. S., Conroy, C., & Wechsler, R. H. 2010, *ApJ*, 717, 379
- Behroozi, P. S., Wechsler, R. H., & Conroy, C. 2013, *ApJ*, 770, 57
- Benson, A. J. et al. 2013, *MNRAS*, 428, 1774
- Bode, P., Ostriker, J. P., & Turok, N. 2001, *ApJ*, 556, 93
- Boyarsky, A., Lesgourgues, J., Ruchayskiy, O., & Viel, M. 2009, *Physical Review Letters*, 102, 201304
- Boylan-Kolchin, M., Bullock, J. S., & Kaplinghat, M. 2011, *MNRAS*, 415, L40
- . 2012, *MNRAS*, 2657
- Breddels, M. A., & Helmi, A. 2013, ArXiv e-prints
- Breddels, M. A., Helmi, A., van den Bosch, R. C. E., van de Ven, G., & Battaglia, G. 2013, *MNRAS*, 433, 3173
- Brooks, A. M., Kuhlen, M., Zolotov, A., & Hooper, D. 2013, *ApJ*, 765, 22
- Buckley, M. R., & Fox, P. J. 2010, *Phys. Rev. D*, 81, 083522
- Chang, J., Macciò, A. V., & Kang, X. 2013, *MNRAS*, 431, 3533
- Choi, J.-H., Weinberg, M. D., & Katz, N. 2009, *MNRAS*, 400, 1247
- Christensen, C., Quinn, T., Governato, F., Stilp, A., Shen, S., & Wadsley, J. 2012, ArXiv e-prints
- Cole, D. R., Dehnen, W., Read, J. I., & Wilkinson, M. I. 2012, ArXiv e-prints
- Collins, M. L. M. et al. 2013a, *ApJ*, 768, 172
- . 2013b, ArXiv e-prints
- . 2011, *MNRAS*, 417, 1170
- Côté, S., Carignan, C., & Freeman, K. C. 2000, *AJ*, 120, 3027
- de Boer, T. J. L., Tolstoy, E., Saha, A., & Olszewski, E. W. 2013, *A&A*, 551, A103
- Del Popolo, A. 2009, *ApJ*, 698, 2093
- Dellenbusch, K. E., Gallagher, III, J. S., Knezek, P. M., & Noble, A. G. 2008, *AJ*, 135, 326
- Destri, C., de Vega, H. J., & Sanchez, N. G. 2013, ArXiv e-prints
- Diemand, J., Kuhlen, M., & Madau, P. 2007, *ApJ*, 667, 859
- Diemand, J., Madau, P., & Moore, B. 2005, *MNRAS*, 364, 367
- D’Onghia, E., Springel, V., Hernquist, L., & Keres, D. 2010, *ApJ*, 709, 1138
- El-Zant, A., Shlosman, I., & Hoffman, Y. 2001, *ApJ*, 560, 636
- Evans, N. W., An, J., & Walker, M. G. 2009, *MNRAS*, 393, L50
- Ferrero, I., Abadi, M. G., Navarro, J. F., Sales, L. V., & Gurovich, S. 2012, *MNRAS*, 425, 2817
- Garrison-Kimmel, S., Rocha, M., Boylan-Kolchin, M., Bullock, J. S., & Lally, J. 2013, *MNRAS*
- Gill, S. P. D., Knebe, A., & Gibson, B. K. 2004, *MNRAS*, 351, 399
- Gilmore, G., Wilkinson, M., Kley, J., Koch, A., Evans, W., Wyse, R. F. G., & Grebel, E. K. 2007, *Nuclear Physics B Proceedings Supplements*, 173, 15
- Gnedin, O. Y., Hernquist, L., & Ostriker, J. P. 1999, *ApJ*, 514, 109
- Goerdt, T., Moore, B., Read, J. I., Stadel, J., & Zemp, M. 2006, *MNRAS*, 368, 1073
- Governato, F. et al. 2012, ArXiv e-prints
- Grebel, E. K., & Gallagher, III, J. S. 2004, *ApJ*, 610, L89
- Haardt, F., & Madau, P. 2001, in *Clusters of Galaxies and the High Redshift Universe Observed in X-rays*, ed. D. M. Neumann & J. T. V. Tran
- Hayashi, E., Navarro, J. F., Taylor, J. E., Stadel, J., & Quinn, T. 2003, *ApJ*, 584, 541
- Hayashi, K., & Chiba, M. 2012, *ApJ*, 755, 145
- Hearin, A. P., Zentner, A. R., Berlind, A. A., & Newman, J. A. 2013, *MNRAS*, 433, 659
- Herpich, J., Stinson, G. S., Macciò, A. V., Brook, C., Wadsley, J., Couchman, H. M. P., & Quinn, T. 2013, ArXiv e-prints
- Jardel, J. R., & Gebhardt, K. 2012, *ApJ*, 746, 89
- . 2013, ArXiv e-prints
- Jardel, J. R., Gebhardt, K., Fabricius, M. H., Drory, N., & Williams, M. J. 2013, *ApJ*, 763, 91
- Kang, X., Macciò, A. V., & Dutton, A. A. 2013, *ApJ*, 767, 22
- Kazantzidis, S., Mayer, L., Mastroiello, C., Diemand, J., Stadel, J., & Moore, B. 2004, *ApJ*, 608, 663
- Kirby, E. N., Bullock, J. S., Boylan-Kolchin, M., Kaplinghat, M., & Cohen, J. G. 2014, *MNRAS*
- Klypin, A., Kravtsov, A. V., Valenzuela, O., & Prada, F. 1999, *ApJ*, 522, 82
- Knollmann, S. R., & Knebe, A. 2009, *ApJS*, 182, 608
- Koposov, S. E., Yoo, J., Rix, H.-W., Weinberg, D. H., Macciò, A. V., & Escudé, J. M. 2009, *ApJ*, 696, 2179
- Kowalczyk, K., Lokas, E. L., Kazantzidis, S., & Mayer, L. 2013, *MNRAS*, 431, 2796
- Kravtsov, A. 2010, *Advances in Astronomy*, 2010
- Kravtsov, A. V., Gnedin, O. Y., & Klypin, A. A. 2004, *ApJ*, 609, 482
- Laporte, C. F. P., Walker, M. G., & Peñarrubia, J. 2013, *MNRAS*, 433, L54
- Leauthaud, A. et al. 2012, *ApJ*, 746, 95
- Li, R., Mo, H. J., Fan, Z., Yang, X., & Bosch, F. C. v. d. 2013, *MNRAS*, 430, 3359
- Libeskind, N. I., Di Cintio, A., Knebe, A., Yepes, G., Gottlöber, S., Steinmetz, M., Hoffman, Y., & Martínez-Vaquero, L. A. 2013, *PASA*, 30, 39
- Libeskind, N. I., Knebe, A., Hoffman, Y., Gottlöber, S., & Yepes, G. 2011, *MNRAS*, 418, 336
- Lora, V., Grebel, E. K., Sanchez-Salcedo, F. J., & Just, A. 2013, ArXiv e-prints
- Lovell, M. R. et al. 2012, *MNRAS*, 420, 2318
- Lovell, M. R., Frenk, C. S., Eke, V. R., Jenkins, A., Gao, L., & Theuns, T. 2013, ArXiv e-prints
- Macciò, A. V., & Fontanot, F. 2010, *MNRAS*, 404, L16
- Macciò, A. V., Paduroiu, S., Anderhalden, D., Schneider, A., & Moore, B. 2012a, *MNRAS*, 424, 1105
- Macciò, A. V., Stinson, G., Brook, C. B., Wadsley, J., Couchman, H. M. P., Shen, S., Gibson, B. K., & Quinn, T. 2012b, *ApJ*, 744, L9
- Madau, P., Diemand, J., & Kuhlen, M. 2008, *ApJ*, 679, 1260
- Martinez, G. D. 2013, ArXiv e-prints
- Mateo, M. L. 1998, *ARA&A*, 36, 435
- McConnachie, A. W. 2012, *AJ*, 144, 4
- McGaugh, S. S., de Blok, W. J. G., Schombert, J. M., Kuzio de Naray, R., & Kim, J. H. 2007, *ApJ*, 659, 149
- Moore, B., Diemand, J., Madau, P., Zemp, M., & Stadel, J. 2006, *MNRAS*, 368, 563
- Moore, B., Ghigna, S., Governato, F., Lake, G., Quinn, T., Stadel, J., & Tozzi, P. 1999, *ApJ*, 524, L19
- Moster, B. P., Naab, T., & White, S. D. M. 2012, ArXiv e-prints
- Muñoz, R. R., Majewski, S. R., & Johnston, K. V. 2008, *ApJ*, 679, 346
- Nichols, M., & Bland-Hawthorn, J. 2013, *ApJ*, 775, 97
- Nierenberg, A. M., Treu, T., Menci, N., Lu, Y., & Wang, W. 2013, *ApJ*, 772, 146
- Oh, S.-H., Brook, C., Governato, F., Brinks, E., Mayer, L., de Blok, W. J. G., Brooks, A., & Walter, F. 2011, *AJ*, 142, 24
- Okamoto, T., Gao, L., & Theuns, T. 2008, *MNRAS*, 390, 920
- Oman, K. A., Hudson, M. J., & Behroozi, P. S. 2013, *MNRAS*, 431, 2307
- Ostriker, J. P., Spitzer, Jr., L., & Chevalier, R. A. 1972, *ApJ*, 176, L51
- Papastergis, E., Martin, A. M., Giovanelli, R., & Haynes, M. P. 2011, *ApJ*, 739, 38

- Peñarrubia, J., Benson, A. J., Walker, M. G., Gilmore, G., McConnachie, A. W., & Mayer, L. 2010, *MNRAS*, 406, 1290
- Peñarrubia, J., McConnachie, A. W., & Navarro, J. F. 2008, *ApJ*, 672, 904
- Peñarrubia, J., Pontzen, A., Walker, M. G., & Koposov, S. E. 2012, *ApJ*, 759, L42
- Peter, A. H. G., Rocha, M., Bullock, J. S., & Kaplinghat, M. 2013, *MNRAS*, 430, 105
- Polisensky, E., & Ricotti, M. 2013, *ArXiv e-prints*
- Pontzen, A., & Governato, F. 2012, *MNRAS*, 421, 3464
- Rashkov, V., Madau, P., Kuhlen, M., & Diemand, J. 2012, *ApJ*, 745, 142
- Read, J. I., & Gilmore, G. 2005, *MNRAS*, 356, 107
- Read, J. I., Wilkinson, M. I., Evans, N. W., Gilmore, G., & Kley, J. T. 2006, *MNRAS*, 367, 387
- Richardson, T., & Fairbairn, M. 2013, *ArXiv e-prints*
- Rocha, M., Peter, A. H. G., Bullock, J. S., Kaplinghat, M., Garrison-Kimmel, S., Oñorbe, J., & Moustakas, L. A. 2013, *MNRAS*, 430, 81
- Rodríguez-Puebla, A., Avila-Reese, V., & Drory, N. 2013, *ApJ*, 773, 172
- Romano-Díaz, E., Shlosman, I., Heller, C., & Hoffman, Y. 2010, *ApJ*, 716, 1095
- Sales, L. V., Navarro, J. F., Abadi, M. G., & Steinmetz, M. 2007a, *MNRAS*, 379, 1475
- . 2007b, *MNRAS*, 379, 1464
- Sales, L. V., Wang, W., White, S. D. M., & Navarro, J. F. 2013, *MNRAS*, 428, 573
- Sawala, T., Scannapieco, C., & White, S. 2012, *MNRAS*, 420, 1714
- Schewtschenko, J. A., & Macciò, A. V. 2011, *MNRAS*, 413, 878
- Schneider, A., Anderhalden, D., Maccio, A., & Diemand, J. 2013, *ArXiv e-prints*
- Shao, S., Gao, L., Theuns, T., & Frenk, C. S. 2013, *MNRAS*, 430, 2346
- Shen, S., Wadsley, J., & Stinson, G. 2010, *MNRAS*, 403, 1043
- Simon, J. D., & Geha, M. 2007, *ApJ*, 670, 313
- Spergel, D. N., & Steinhardt, P. J. 2000, *Physical Review Letters*, 84, 3760
- Springel, V. et al. 2008, *MNRAS*, 391, 1685
- Stadel, J. G. 2001, PhD thesis, UNIVERSITY OF WASHINGTON
- Stinson, G., Seth, A., Katz, N., Wadsley, J., Governato, F., & Quinn, T. 2006, *MNRAS*, 373, 1074
- Strigari, L. E., Frenk, C. S., & White, S. D. M. 2010, *MNRAS*, 408, 2364
- Taylor, J. E., & Babul, A. 2001, *ApJ*, 559, 716
- Teyssier, M., Johnston, K. V., & Kuhlen, M. 2012a, *MNRAS*, 426, 1808
- Teyssier, R., Pontzen, A., Dubois, Y., & Read, J. 2012b, *ArXiv e-prints*
- Tikhonov, A. V., Gottlöber, S., Yepes, G., & Hoffman, Y. 2009, *MNRAS*, 399, 1611
- Tollerud, E. J. et al. 2012, *ApJ*, 752, 45
- Tollerud, E. J., Bullock, J. S., Strigari, L. E., & Willman, B. 2008, *ApJ*, 688, 277
- Tollerud, E. J., Geha, M. C., Vargas, L. C., & Bullock, J. S. 2013, *ApJ*, 768, 50
- Tonini, C., Lapi, A., & Salucci, P. 2006, *ApJ*, 649, 591
- Tulin, S., Yu, H.-B., & Zurek, K. M. 2013, *Phys. Rev. D*, 87, 115007
- Vera-Ciro, C. A., Helmi, A., Starkenburg, E., & Breddels, M. A. 2013, *MNRAS*, 428, 1696
- Viel, M., Becker, G. D., Bolton, J. S., & Haehnelt, M. G. 2013, *Phys. Rev. D*, 88, 043502
- Vogelsberger, M., & Zavala, J. 2013, *MNRAS*, 430, 1722
- Vogelsberger, M., Zavala, J., & Loeb, A. 2012, *MNRAS*, 423, 3740
- Wadepuhl, M., & Springel, V. 2011, *MNRAS*, 410, 1975
- Wadsley, J. W., Stadel, J., & Quinn, T. 2004, *New Astronomy*, 9, 137
- Walker, M. G., Mateo, M., Olszewski, E. W., Peñarrubia, J., Wyn Evans, N., & Gilmore, G. 2009, *ApJ*, 704, 1274
- Walker, M. G., & Peñarrubia, J. 2011, *ApJ*, 742, 20
- Walsh, S. M., Willman, B., & Jerjen, H. 2009, *AJ*, 137, 450
- Wechsler, R. H., Bullock, J. S., Primack, J. R., Kravtsov, A. V., & Dekel, A. 2002, *ApJ*, 568, 52
- Weisz, D. R. et al. 2011, *ApJ*, 739, 5
- Wojtak, R., Gottlöber, S., & Klypin, A. 2013, *MNRAS*, 434, 1576
- Wolf, J., & Bullock, J. S. 2012, *ArXiv e-prints*
- Wolf, J., Martinez, G. D., Bullock, J. S., Kaplinghat, M., Geha, M., Muñoz, R. R., Simon, J. D., & Avedo, F. F. 2010, *MNRAS*, 406, 1220
- Zavala, J., Vogelsberger, M., & Walker, M. G. 2013, *MNRAS*, 431, L20
- Zhao, D. H., Jing, Y. P., Mo, H. J., & Börner, G. 2003, *ApJ*, 597, L9
- Zolotov, A. et al. 2012, *ApJ*, 761, 71